Materials and Design 156 (2018) 229–241

Contents lists available at ScienceDirect

Materials and Design

journal homepage: www.elsevier.com/locate/matdes

Creep of closed-cell aluminum foams: Effects of imperfections and predictive modeling

Bin Han [a,b,c], Run-Pei Yu [b,d], Qian-Cheng Zhang [b,d], Hua-Jian Gao [c], Qi Zhang [a,*], Tian Jian Lu [b,d,**], Bing-Heng Lu [a]

[a] School of Mechanical Engineering, Xi'an Jiaotong University, Xi'an 710049, China
[b] MOE Key Laboratory for Multifunctional Materials and Structures, Xi'an Jiaotong University, Xi'an 710049, China
[c] School of Engineering, Brown University, Providence, RI 02912, USA
[d] State Key Laboratory for Strength and Vibration of Mechanical Structures, Xi'an Jiaotong University, Xi'an 710049, China

HIGHLIGHTS

- Effects of five types of morphological imperfections on the creep of closed-cell foams are evaluated.
- A refined creep model of tetrakaidecahedral closed-cell foams is proposed.
- Cell-wall imperfections greatly speed up the creep rate of closed-cell foams.
- Interactions among different random imperfections are small and can be neglected.

GRAPHICAL ABSTRACT

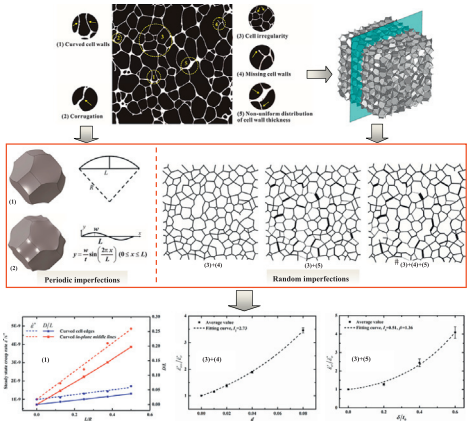

ARTICLE INFO

Article history:
Received 28 March 2018
Received in revised form 11 June 2018
Accepted 27 June 2018
Available online 30 June 2018

Keywords:
Imperfections
Steady state creep
Closed-cell foam
Finite element modeling
Theoretical modeling

ABSTRACT

The influence of five different types of morphological imperfection – curved cell wall, corrugation, cell shape irregularity, missing cell walls and non-uniform distribution of cell wall thickness – on steady state creep of closed-cell aluminum foams is systematically studied under uniaxial compressive loading. A refined theoretical model is developed to predict the steady state creep rate of idealized tetrakaidecahedral (TKD) closed-cell foams. Based upon the TKD model, finite element modeling is also carried out. The presence of imperfections usually leads to significant increase in steady state creep rate. The creep rate increases linearly with the degree of cell shape irregularity and the curvature of curved cell walls, while increases as a power law function of the area fraction of missing cell walls and the dispersion degree of non-uniform distributed cell wall thickness. The combined effect of three different random defects—cell shape irregularity, missing cell walls and non-uniform distribution of cell wall thickness—causes more drastic increase in creep rate than any single or dual imperfections. Interactions among the three are small and can be neglected. Finally, an empirical formula of steady state creep rate is proposed to give a good prediction for closed-cell foams with random imperfections.

* Corresponding author.
** Correspondence to: T.J. Lu, MOE Key Laboratory for Multifunctional Materials and Structures, Xi'an Jiaotong University, Xi'an 710049, China.
E-mail addresses: henryzhang@mail.xjtu.edu.cn, (Q. Zhang), tjlu@mail.xjtu.edu.cn (T.J. Lu).

https://doi.org/10.1016/j.matdes.2018.06.050
0264-1275/

1. Introduction

Closed-cell metallic foams exhibit great performance in energy absorption, damping, acoustic and thermal insulation, as well as electromagnetic shielding [1–3]. They are also well suited for high temperature applications, such as the core of load-bearing sandwich structures in high temperature environments (e.g., gas reactor, combustion chamber and modern steam turbine), owing to their better resistance to oxidation than polymeric foams and much better toughness, thermal conductivity and thermal shock resistance than ceramic foams [4]. For long-term applications, however, the susceptibility to creep deformation must be taken into consideration in determining the service life when a metallic foam is loaded at temperature greater than about 1/3 to 1/2 of the melting point of its parent material. At present, whereas numerous investigations have been performed to study the creep behaviors of cellular metals, mainly focusing on honeycombs and open-cell foams [4–15], only a few studies have addressed the creep of closed-cell metallic foams.

Based upon an idealized cubic cell, Gibson and Ashby [16,17] developed a power-law creep model for both open-cell and closed-cell foams, assuming that the major contributions to macroscopic creep stem from the creep bending of transversely loaded struts and the creep stretching of cell membrane. To access the validity of this model, Andrews et al. [17,18] performed creep experiments on open-cell (Duocel) and closed-cell (Alporas) aluminum foams. While the experimental results for the open-cell foam were in excellent agreement with the model predictions, the creep resistance of the closed-cell foam was considerably lower than that predicted. It was argued that the inhomogeneous microstructure of the closed-cell foam led to a broad distribution of stresses within the sample, thus causing some cell walls to enter the power-law breakdown (PLB) regime [18]. Subsequently, Zhang et al. [19] examined the microstructure of an Alporas foam both before and after creep deformation, and found that the microstructure development was rather inhomogeneous during creep, due at least in part to the complicated distribution of the applied stress in the foam. They indicated that local stresses more than an order of magnitude higher than the average stress were present during creep. Haag et al. [20] found experimentally that closed-cell foams exhibited a higher creep strain rate and a higher stress exponent than those predicted by the Gibson-Ashby model for regular (idealized) foams, and suggested that the discrepancies were probably due to the combined effects of primary creep and localized PLB within the cell walls as well as geometric instabilities developing during the course of deformation.

Most commercially available metallic foams exhibit a variety of processing-induced morphological imperfections, including curved and wrinkled cell walls, non-uniform wall thickness, cell wall misalignments, broken cell walls, missing cells, and random dispersion of cell size [21–23]. These imperfections can have remarkable influence on the mechanical properties of the foams [24–27]. In particular, the effect of imperfections on the creep behavior has been investigated. For instance, Andrews and Gibson [6] studied the effect of cell shape variation, cell size distribution and cell wall curvature on the creep strain rate of 2D (two-dimensional) cellular solids, and found that the three types of imperfection can all accelerate creep. Huang and Gibson [7] investigated the creep behavior of 3D (three-dimensional) Voronoi open-cell foams with missing struts, and concluded that the removal of only a few percent of struts would increase the creep strain rate by one or two orders of magnitude. Lin and Huang [28] evaluated the effects of solid distribution along cell edges on the creep strain rates of 2D hexagonal honeycombs, and found that there existed an optimal distribution minimizing the creep strain rate. More recently, based 2D honeycomb and 3D tetrakaidecahedral strut models, Su et al. [13] studied the effect of missing cell struts on steady state creep of cellar materials and proposed a theoretical model to predict the creep rate. However, existing studies only addressed how the creep behavior of regular honeycombs and open-cell foams is influenced by the presence of imperfections. There is yet a study concerning the effects of imperfections on the creep response of 3D closed-cell metallic foams.

The present study aims to investigate the effects of a variety of morphological imperfections on uniaxial steady state creep of high porosity closed-cell aluminum foams. As clearly shown in Fig. 1, the imperfections considered include curved cell walls, corrugation, cell shape irregularity, missing cell walls, and non-uniform distribution of cell wall thickness, which are closed related to the liquid-state foaming process of Alporas foams [23,29]. Firstly, a theoretical model is developed with a semi-analytical formulation to predict the steady state creep rate of idealized tetrakaidecahedral (TKD) closed-cell foams. Subsequently, the effects of periodic imperfections on creep are quantified using finite element (FE) simulations. Lastly, the effects of random imperfections are also numerically investigated and their interactions are discussed, with the steady creep rate predicted by empirical equations.

2. Creep of closed-cell foams with TKD cells

According to their pore shapes, closed-cell aluminum (Al) foams fabricated via the method of melt-foaming may be classified into three categories: polygonal pores with high porosity (85%–95%), sphere-like pores with intermediate porosity (70%–80%), and spherical pores with relatively low porosity (<70%) [30]. Most of the commercially available closed-cell Al foams (e.g., Alporas foam) possess a low relative density <0.15 and hence their cellular morphology is dominated by polygonal pores.

Several space-filling unit cells, including cubic, tetrahedral, dodecahedral and TKD cells, have been employed to develop closed-form structure-property relations of 3D cellular solids [31]. Among these polyhedron cells, the TKD cell is known to be the only polyhedron that can be packed with identical units to fill space with nearly minimum surface energy [32–34], which is closest to the realistic pore shape of high porosity closed-cell aluminum foams. Therefore, in the present study, the TKD cell with uniform cell wall thickness is used as an idealized model to study the creep behavior of closed-cell foams.

2.1. Theoretical models for TKD closed-cell foams

Built upon the cubic unit cell, the Gibson-Ashby model [16,17] gave the following uniaxial steady state creep rate $\dot{\varepsilon}^*$ of closed-cell foams as a function of relative density $\overline{\rho}$:

$$\frac{\dot{\varepsilon}^*}{\dot{\varepsilon}_0} = f(\overline{\rho})\left(\frac{\sigma^*}{\sigma_0}\right)^n \tag{1}$$

where $\dot{\varepsilon}_0$, σ_0, n are the temperature-dependent creep constants of cell wall material, and σ^* is the uniaxial stress applied on the foam. The coefficient function $f(\overline{\rho})$ is expressed as:

$$f(\overline{\rho}) = \left\{\frac{1}{1.7}\left(\frac{n+2}{0.6}\right)^{\frac{1}{n}}\left(\frac{n}{2n+1}\right)(\phi\overline{\rho})^{\frac{3n+1}{2n}} + \frac{2}{3}(1-\phi)\overline{\rho}\right\}^{-n} \tag{2}$$

in which ϕ is the fraction of solid contained in cell edges/struts.

Different from the cubic-cell model, the representative volume element (RVE) of TKD closed-cell foams on a body-centered cubic (BCC) lattice consists of 6 square faces, 12 quarter-square (isosceles triangle) faces, 8 hexagonal faces and 36 struts, as shown in Fig. 2. Faces with thickness t_f constitute cell walls, while struts with thickness t_e and length L denote cell edges. In the current study, the cross-section of the struts is assumed to be square [7,13]. Due to the sharing of boundaries with neighboring RVEs, the thickness of the 6 square faces and the cross-sectional area of the corresponding 24 struts in the RVE model are both halved.

Since the bending of struts has been found to be the dominant creep mechanism for open-cell foams with low relative densities (<0.20) [10],

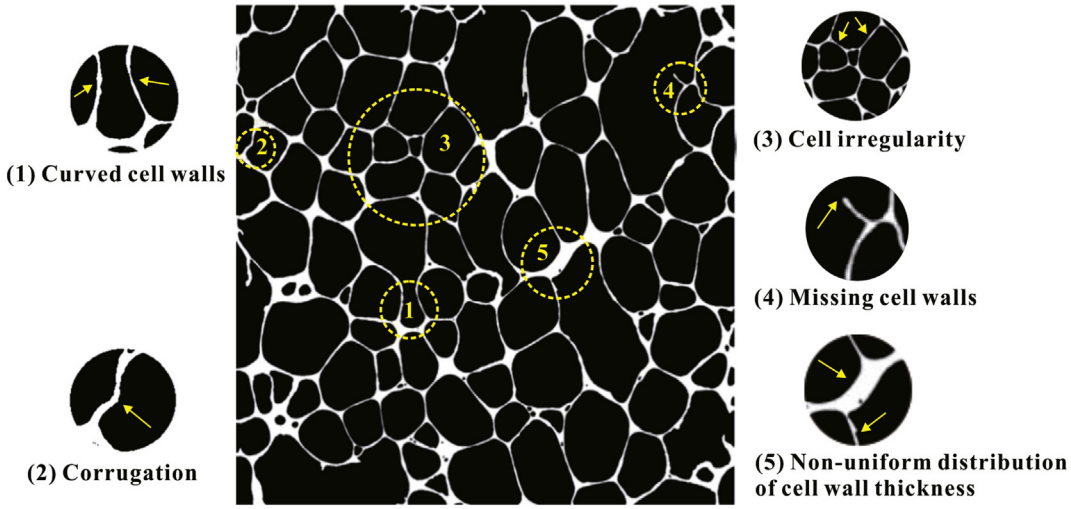

Fig. 1. Five different types of cell-wall imperfection considered: (1) curved cell walls, (2) corrugation, (3) cell irregularity, (4) missing cell walls, and (5) non-uniform distribution of cell wall thickness. This picture is taken from an X-ray CT slice image of a closed-cell aluminum foam (Alporas™) [23].

it is reasonable to assume that the major contributions to macroscopic creep of the present TKD closed-cell foams (with a relative density <0.15) come from the bending of cell edges/struts and the stretching of cell walls/faces. Therefore, the work rate $\dot{W}$ produced by the uniaxial compressive stress σ^* (exerted on the top and bottom surfaces) is given by:

$$\dot{W} = \dot{D}_b + \dot{D}_{st} \tag{3}$$

where $\dot{D}_b$ and $\dot{D}_{st}$ represent the rate of energy dissipation as a result of creep bending of cell edges and creep stretching of cell walls, respectively.

Firstly, the rate of energy dissipation and the creep rate of struts are derived. It is assumed that a pair of concentrated compressive forces $4P_{strut}$ is applied on the rigid vertices of the struts in the upper/bottom square faces (Fig. 2). Owing to symmetry, only one quarter of the TKD struts (named from S1 to S12) needs to be analyzed, as shown in Fig. 3.

The rate of energy dissipation of the i-th strut ($i = 1, 2, \ldots, 12$) caused by creep bending can be calculated from:

$$\dot{D}_i = \int_0^L M_i(x) \cdot \dot{\kappa}_i dx \tag{4}$$

where $M_i(x)$ is the bending moment acting at any cross section of the i-th strut with a distance x measured from one end of the same strut (detailed expression illustrated as a function of P_{strut} in Table 1 of ref. [35]), and $\dot{\kappa}_i$ is the change rate of curvature which can be calculated by [17]:

$$\dot{\kappa}_i = \dot{\varepsilon}_0 \left[\left(\frac{2n+1}{2n} \right) \frac{M_i(x)}{t_e \sigma_0} \right]^n \left(\frac{2}{t_e} \right)^{2n+1} \tag{5}$$

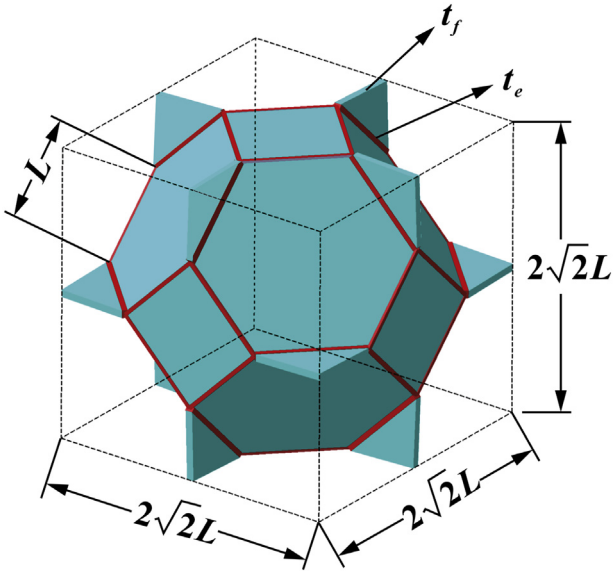

Fig. 2. Representative volume element (RVE) model of TKD closed-cell foam. Red lines represent struts, and green faces denote cell walls.

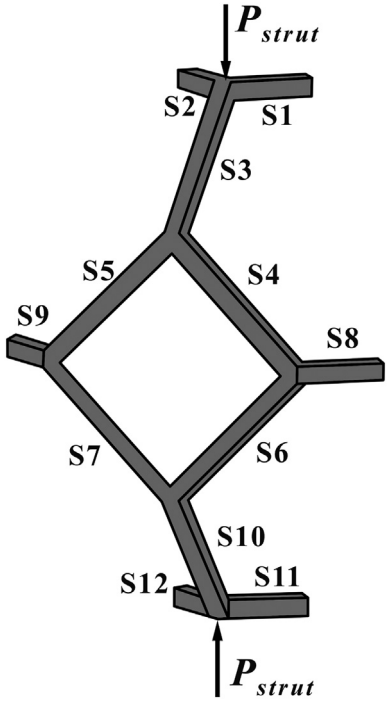

Fig. 3. Schematic of a quarter of TKD strut cell under compression.

Hence, the rate of energy dissipation of each strut can be calculated as:

$$\begin{cases} \dot{D}_1 = \dot{D}_2 = \dot{D}_{11} = \dot{D}_{12} = 2^{n-2} \cdot \left(\dfrac{2n+1}{n}\right)^n \cdot P_{strut}^{n+1} \cdot \dfrac{\dot{\varepsilon}_0}{\sigma_0^n} \cdot \dfrac{L^{n+2}}{t_e^{3n+1}} \\ \dot{D}_3 = \dot{D}_{10} = \dfrac{\left(\sqrt{2}\right)^{n+1}}{(n+2)\cdot 2^{2n+2}} \cdot \left(\dfrac{2n+1}{n}\right)^n \cdot P_{strut}^{n+1} \cdot \dfrac{\dot{\varepsilon}_0}{\sigma_0^n} \cdot \dfrac{L^{n+2}}{t_e^{3n+1}} \\ \dot{D}_4 = \dot{D}_5 = \dot{D}_6 = \dot{D}_7 = \dfrac{2^{n+1} + \left(3\sqrt{2}\right)^{n+1}}{4(n+2)} \cdot \left(\dfrac{2n+1}{n}\right)^n \cdot P_{strut}^{n+1} \cdot \dfrac{\dot{\varepsilon}_0}{\sigma_0^n} \cdot \dfrac{L^{n+2}}{t_e^{3n+1}} \\ \dot{D}_8 = \dot{D}_9 = \dfrac{\left(\sqrt{2}\right)^{n+1}}{2^{2n+3}} \cdot \left(\dfrac{2n+1}{n}\right)^n \cdot P_{strut}^{n+1} \cdot \dfrac{\dot{\varepsilon}_0}{\sigma_0^n} \cdot \dfrac{L^{n+2}}{t_e^{3n+1}} \end{cases} \tag{6}$$

The rate of total energy dissipation of the 36 struts in RVE is thus given by:

$$\begin{aligned} \dot{D}_b &= 4\sum_{i=1}^{12} \dot{D}_i = 4\left(4\dot{D}_1 + 2\dot{D}_3 + 4\dot{D}_4 + 2\dot{D}_8\right) \\ &= \left[2^{n+2} + \frac{\left(\sqrt{2}\right)^{n+1}}{(n+2)\cdot 2^{2n-1}} + \frac{2^{n+3}}{(n+2)} + \frac{4\left(3\sqrt{2}\right)^{n+1}}{(n+2)} + \frac{\left(\sqrt{2}\right)^{n+1}}{2^{2n}}\right] \\ &\quad \times \left(\frac{2n+1}{n}\right)^n \cdot P_{strut}^{n+1} \cdot \frac{\dot{\varepsilon}_0}{\sigma_0^n} \cdot \frac{L^{n+2}}{t_e^{3n+1}} \end{aligned} \tag{7}$$

Moreover, the work rate $\dot{W}_{strut}$ produced by P_{strut} can be expressed as:

$$\dot{W}_{strut} = 4P_{strut} \cdot 2\sqrt{2}L \cdot \dot{\varepsilon}_b^* = 8\sqrt{2}P_{strut} \cdot \dot{\varepsilon}_b^* \cdot L \tag{8}$$

Eventually, by equating $\dot{W}_{strut}$ to $\dot{D}_b$, the macroscopic creep rate of the TKD strut-cell model $\dot{\varepsilon}_b^*$ can be derived as:

$$\begin{aligned} \dot{\varepsilon}_b^* = &\left[\sqrt{2}\cdot 2^{n-2} + \frac{\left(\sqrt{2}\right)^n}{(n+2)\cdot 2^{2n+2}} + \frac{2^n}{\sqrt{2}(n+2)} + \frac{\left(3\sqrt{2}\right)^{n+1}}{2\sqrt{2}(n+2)} + \frac{\left(\sqrt{2}\right)^n}{2^{2n+3}}\right] \\ &\varepsilon_0 \left(\frac{2n+1}{n}\right)^n \cdot \left(\frac{P_{strut}}{L^2\sigma_0}\right)^n \cdot \left(\frac{L}{t_e}\right)^{3n+1} \end{aligned} \tag{9}$$

Secondly, the rate of energy dissipation and the creep rate of cell walls are calculated. The faces of a closed-cell foam carry membrane stresses when the foam deforms. As all the faces are flat, the membrane stress σ_f^i of each face scales as $\sigma_f^* L/t_f$ (where σ_f^* is the average effective stress exerted on the whole face model) with a scale factor of β_i [17], causing the i-th face to strain at a rate:

$$\dot{\varepsilon}_f^i = \dot{\varepsilon}_0 \left(\frac{\sigma_f^i}{\sigma_0}\right)^n = \dot{\varepsilon}_0 \left(\beta_i \frac{\sigma_f^*}{\sigma_0} \cdot \frac{L}{t_f}\right)^n \tag{10}$$

Hence, the rate of total energy dissipation caused by the creep stretching of faces can be written as:

$$\dot{D}_{str} = \frac{1}{2}\sum_i \dot{\varepsilon}_f^i \cdot \sigma_f^i \cdot t_f S_f^i = \frac{1}{2}\sum_i \frac{\dot{\varepsilon}_0}{\sigma_0^n}\left(\beta_i \cdot \sigma_f^* \cdot \frac{L}{t_f}\right)^{n+1} \cdot \gamma_i t_f L^2 \tag{11}$$

where S_f^i denotes the area of the i-th face and γ_i is a shape factor ($\gamma_i = S_f^i/t_f L^2$). The work rate $\dot{W}_{face}$ produced by σ_f^* can be calculated as:

$$\dot{W}_{face} = \left(2\sqrt{2}L\right)^2 \sigma_f^* \cdot 2\sqrt{2}L \cdot \dot{\varepsilon}_f^* = 16\sqrt{2}\sigma_f^* \cdot \dot{\varepsilon}_f^* \cdot L^3 \tag{12}$$

Therefore, by equating $\dot{W}_{face}$ to $\dot{D}_{str}$, the macroscopic creep rate of the TKD face-cell model can be obtained as:

$$\dot{\varepsilon}_f^* = \frac{\dot{\varepsilon}_0}{32\sqrt{2}} \cdot \left(\frac{\sigma_f^*}{\sigma_0}\right)^n \cdot \sum_i {\beta_i}^{n+1} \cdot \left(\frac{L}{t_f}\right)^n \cdot \gamma_i \tag{13}$$

Finally, rewriting the work rate of the entire RVE model, one gets

$$\dot{W} = \left(2\sqrt{2}L^2\right)\sigma^* \cdot 2\sqrt{2}L \cdot \dot{\varepsilon}^* = 16\sqrt{2}\sigma^* \cdot \dot{\varepsilon}^* \cdot L^3 \tag{14}$$

In the RVE model, because of deformation compatibility, the steady state creep rates of the cell edges and cell walls should both equal to that of the whole model, i.e., $\dot{\varepsilon}_b^* = \dot{\varepsilon}_f^* = \dot{\varepsilon}^*$. Then, from Eqs. (3), (7), (9), (11), (13) and (14), the steady state creep rate of the TKD closed-cell foam $\dot{\varepsilon}_{TKD}^*$ can be written in the form of Eq. (1), with the corresponding coefficient function $f(\overline{\rho})$ given by:

$$f(\overline{\rho}) = \left\{ \frac{\frac{n}{2n+1} \cdot \left(\frac{t_e}{L}\right)^{\frac{3n+1}{n}}}{2\left[\sqrt{2}\cdot 2^{n-2} + \frac{\left(\sqrt{2}\right)^n}{(n+2)\cdot 2^{2n+2}} + \frac{2^n}{\sqrt{2}(n+2)} + \frac{\left(3\sqrt{2}\right)^{n+1}}{2\sqrt{2}(n+2)} + \frac{\left(\sqrt{2}\right)^n}{2^{2n+3}}\right]^{\frac{1}{n}}} + \left[\frac{32\sqrt{2}}{\sum_i \beta_i^{n+1}\gamma_i}\right]^{\frac{1}{n}} \cdot \frac{t_f}{L} \right\}^{-n} \tag{15}$$

Assume that the thickness of cell edge is equal to that of cell walls/faces, i.e., $t_e = t_f = t$. Regardless of the overlap of the faces and struts, the total volume of solid contained in the RVE model is thence:

$$V_{\text{total}} = \left(6 + 12\sqrt{3}\right)tL^2 + 18t^2L \tag{16}$$

The relative density $\overline{\rho}$ and the fraction of solid contained in the cell edges ϕ can be obtained as:

$$\begin{aligned} \overline{\rho} &= \frac{\left(6+12\sqrt{3}\right)tL^2 + 18t^2L}{16\sqrt{2}L^3} = 1.1837\frac{t}{L} + 0.7955\left(\frac{t}{L}\right)^2, \\ \phi &= \frac{V_{\text{strut}}}{V_{\text{total}}} = \frac{18t^2L}{\left(6+12\sqrt{3}\right)tL^2 + 18t^2L} = \frac{3t}{\left(1+2\sqrt{3}\right)L + 3t} \end{aligned} \tag{17}$$

Then, upon substituting t/L by $\overline{\rho}$ and ϕ, Eq. (16) can be rewritten as:

$$f(\overline{\rho}) = \left[A_1(\phi\overline{\rho})^{\frac{3n+1}{2n}} + A_2(1-\phi)\overline{\rho}\right]^{-n} \tag{18}$$

where the constants A_1 and A_2 are

$$\begin{aligned} A_1 &= \left(\frac{8\sqrt{2}}{9}\right)^{\frac{3n+1}{2n}} \frac{n}{2(2n+1)}\left[\sqrt{2}\cdot 2^{n-2} + \frac{\left(\sqrt{2}\right)^n}{(n+2)\cdot 2^{2n+2}} + \frac{2^n}{\sqrt{2}(n+2)} + \frac{\left(3\sqrt{2}\right)^{n+1}}{2\sqrt{2}(n+2)} + \frac{\left(\sqrt{2}\right)^n}{2^{2n+3}}\right]^{-\frac{1}{n}}, \\ A_2 &= \frac{8\sqrt{2}}{\left(3+6\sqrt{3}\right)}\left(\frac{32\sqrt{2}}{\sum_i \beta_i^{n+1}\gamma_i}\right)^{\frac{1}{n}} \end{aligned} \tag{19}$$

Because of the complexity of the TKD face-cell model, it is difficult to derive an analytical expression of the scale factor of membrane stress, β_i. However, the constant A_2 can be approximately determined based on the fitting of the simulated results, as illustrated later.

It is noteworthy that the creep coefficient function $f(\overline{\rho})$ of the Gibson-Ashby model, i.e., Eq. (2), can also be written in the same form of Eq. (18), with different expressions of A_1 and A_2. This suggests that the constants A_1 and A_2 are determined by the base material (i.e., the stress exponent n) and the geometry of closed-cell foam models.

2.2. Finite element modeling

To validate the above theoretical model, the finite element (FE) analysis code ABAQUS is adopted to simulate the creep behaviors of both the TKD strut-cell model and the TKD closed-cell model. As shown in Fig. 4, a periodic unit consisting of $8 \times 8 \times 8$ RVE cells for TKD strut-cell or closed-cell model is analyzed, with periodic boundary conditions assigned on all the 6 faces of the structure to simulate a foam of infinite dimensions. The strut-cell model is meshed using the linear Timoshenko beam elements (B31) with 8 elements along each strut, while the closed-cell model is meshed using the 4-node reduced integration shell element S4R with an element size of about $L/8$. The concentrated compressive force P_{strut} is exerted on all vertices of the upper and bottom faces for the TKD strut-cell model. For the TKD closed-cell model, the nominal compressive stress σ^* is exerted on the analytical rigid surfaces.

The base material of the cell walls and struts is assumed to follow power law creep $\dot{\varepsilon} = \dot{\varepsilon}_0(\sigma/\sigma_0)^n$ with $n = 6.25$, $\dot{\varepsilon}_0/\sigma_0^n = 5.6 \times 10^{-17}$ $\mathrm{MPa}^{-6.25} \cdot \mathrm{s}^{-1}$, Young's modulus $E = 65.5\mathrm{GPa}$, and Poisson ratio $\nu = 0.33$, which are representative of the cell wall material of Alporas closed-cell aluminum foams at 300°C [20].

2.3. Comparison with theoretical, numerical and experimental results

As shown in Table 1, good agreement is achieved between FE simulation results and theoretical model predictions (i.e., Eq. (9)) for steady creep strain rate $\dot{\varepsilon}_b^*$ of the TKD strut-cell model.

Subsequently, FE simulations for the creep of TKD closed-cell models having various relative densities under constant compressive stress $\sigma^* = 0.4$ MPa are carried out to determine the fitting value of constant A_2 in Eq. (19), as shown in Fig. 5. It is found that the expression of Eq. (18) with $A_1 = 0.102$ and $A_2 = 0.332$ for TKD closed-cell models yields a good match with the simulation results. In contrast, the steady state creep rate as predicted by the Gibson-Ashby model (i.e., Eq. (2)) is two orders of magnitude lower than that of the TKD closed-cell model. This indicates that the geometrical features of the cells have a great influence on the creep response of closed-cell aluminum foams.

As shown in Table 2, the predictions by the present TKD closed-cell model and the Gibson-Ashby model are both compared with the experimental results of Alporas foams [18]. Whereas the TKD model gives much better predictions than the Gibson-Ashby model, both predictions greatly underestimate the steady state creep rate of Alporas foams. It is supposed that the large discrepancy between theory and experiment is caused by processing-induced morphological imperfections which are inevitably present in Alporas foams, as shown in Fig. 1. Consequently, in the sections to follow, the effects of five different types of cell-wall imperfections, i.e., curved cell walls, corrugation, cell shape irregularity, missing cell walls, and non-uniform distribution of wall thickness, on the creep of closed-cell aluminum foams are quantified using FE simulations. For convenience of comparison, the uniaxial compressive stress is taken as $\sigma^* = 0.4$ MPa in all the following simulations. Periodic boundary conditions are employed for each calculation.

3. Periodic imperfections

The cell walls of conventional closed-cell aluminum foams with low relative density are often curved or corrugated, which usually results from pressure differences between cells in the liquid foam before solidification and mechanical manipulations of the foam during or immediately following solidification [36]. Such imperfections often deteriorate the mechanical properties of the foam [36,37]. As periodic imperfections, curved walls and corrugation are studied in this section for the creep of regular TKD closed-cell models, with the relative density fixed at 0.088. For models with curved or corrugated cell walls, finer meshing is needed to guarantee numerical convergence.

3.1. Curved cell walls

3.1.1. Model description

As shown in Fig. 6, the curved cell walls can be determined by the curvature of either the cell edges or the middle lines (referred to as *in-plane middle lines*) connecting the midspan of one cell edge to the midspan of the opposite cell edge, with a uniform curvature radius of R. Both methods are employed to construct the curved cell walls.

With the first method, all the cell edges can be classified into three groups, which are marked using three different colors—red, yellow and blue—in Fig. 6a. For instance, the 12 *red* cell edges initially parallel to square face A are curved and perpendicular to Plane A, with 6 parallel edges curved in one/positive direction, and the other 6 in the opposite/negative direction to avoid corner distortion of the square faces. The same method is used for other 12 *yellow* and 12 *blue* cell edges. With all the curved cell edges determined, the curved TKD cell-strut model is constructed as shown in Fig. 6b; subsequently, the corresponding cell walls can be obtained with automatic formation of smooth surfaces by ABAQUS (see Fig. 6c).

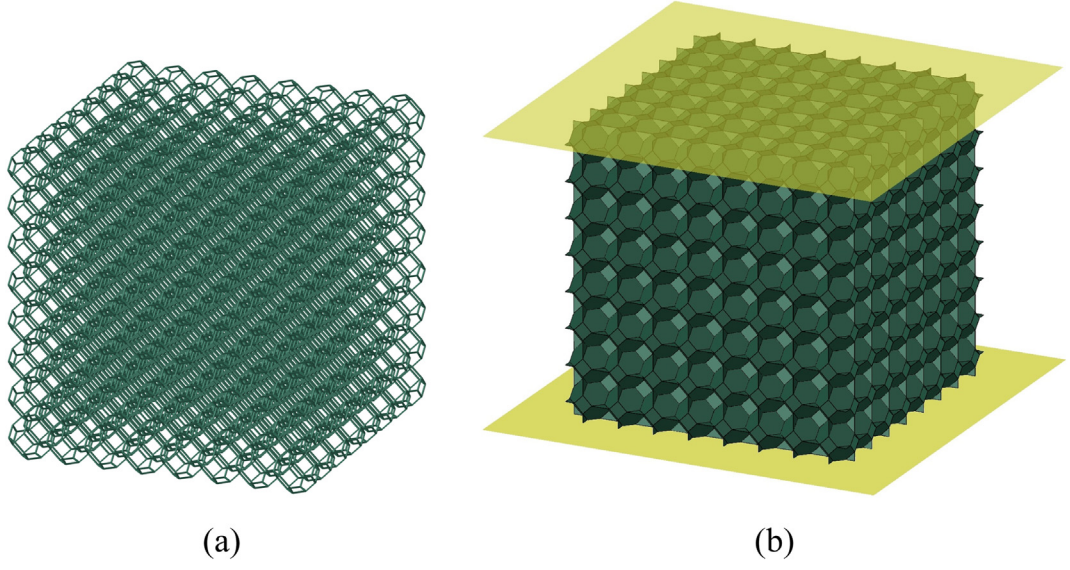

Fig. 4. Periodic unit consisting of $8 \times 8 \times 8$ RVE cells for (a) TKD strut-cell and (b) TKD closed-cell model under constant compressive load.

Table 1
Steady state creep rate for TKD strut-cell model: Comparison between FE simulations and theoretical model predictions[a].

$P_{strut}/L^2(\times 10^{-3}$ MPa)	t_e/L	$\dot{\varepsilon}^*_{b-Anl}$ (s^{-1})	$\dot{\varepsilon}^*_{b-FE}$ (s^{-1})	Δ (%)
10	0.1	1.91×10^{-4}	2.02×10^{-4}	−5.4
8	0.1	4.73×10^{-5}	5.01×10^{-5}	−5.6
6	0.1	7.83×10^{-6}	8.29×10^{-6}	−5.6
4	0.1	6.21×10^{-7}	6.59×10^{-7}	−5.8
4	0.09	4.98×10^{-6}	5.21×10^{-6}	−4.4
4	0.08	5.09×10^{-5}	5.28×10^{-5}	−3.6
4	0.07	7.12×10^{-4}	7.36×10^{-4}	−3.3

[a] $\dot{\varepsilon}^*_{b-Anl}$ and $\dot{\varepsilon}^*_{b-FE}$ refer to the steady state creep rate $\dot{\varepsilon}^*_b$ obtained from Eq. (9) and FE simulations, respectively. Δ denotes the percentage error of $\dot{\varepsilon}^*_{b-Anl}$ relative to $\dot{\varepsilon}^*_{b-FE}$.

With the second method, all the cell edges remain straight. Only the *in-plane middle lines* in each square and hexagonal cell face are curved and normal to the initially flat cell walls, as shown in Fig. 6d–e. When all the curved *in-plane middle lines* are determined, the curved cell walls are obtained via smooth approximation by ABAQUS, as shown in Fig. 6f.

The FE models for TKD closed-cell foams with curved cell walls are constructed with $8 \times 8 \times 8$ RVE cells, with the same material and boundary conditions as above. The dimensionless curvature parameter L/R varies between 0 and 0.5 for models constructed using either curved cell edges or curved *in-plane middle lines*.

3.1.2. Results and discussion

The steady state creep rate $\dot{\varepsilon}^*$ of foam models with curved cell walls is plotted as a function of L/R in Fig. 7. For both foam models, $\dot{\varepsilon}^*$ increases linearly with L/R. For the model constructed with curved cell edges, $\dot{\varepsilon}^*$ increases by about 70% as L/R is increased to 0.5; whereas for the model determined by curved *in-plane middle lines*, $\dot{\varepsilon}^*$ increases by a factor of nearly 4 at $L/R = 0.5$. This indicates that the effect of curved *in-plane middle lines* have a greater influence on the creep of closed-cell foams than the curved cell edges, because the former usually leads to larger out-of-plane deflections than the latter. With the maximum out-of-plane deflection D in hexagonal faces as a function of L/R added to Fig. 7, it can be seen that at $L/R = 0.5$, D is $0.197L$ and $0.0367L$ for models constructed with curved cell edges and curved *in-plane middle lines*, respectively. In other words, cell walls with curved cell edges are more prone to deform than those determined by curved *in-plane middle lines*, resulting in sharper increase of steady state creep rate.

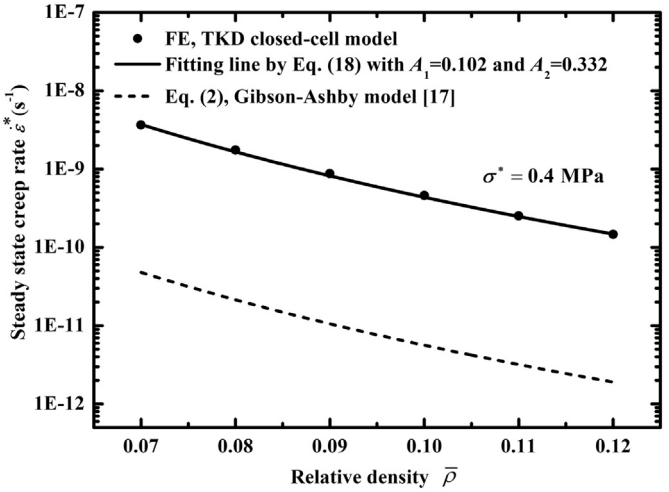

Fig. 5. Steady state creep rate of TKD closed-cell model as a function of relative density.

3.2. Corrugation of cell walls

The corrugation of cell walls is defined by corrugated cell edges, as shown in Fig. 8, which is sinusoidal with a wavelength of L. In terms of local coordinates, the geometry of each corrugated cell edge is defined by:

$$y = \frac{w}{t} \sin\left(\frac{2\pi x}{L}\right) \qquad (0 \le x \le L) \tag{20}$$

where w is the corrugation amplitude at mid-edge. Similar to the definition of curved cell walls determined by curved cell edges, the corrugated cell edges are oriented perpendicular to the initially square face. Once the cell edges are determined, the corrugated cell walls are obtained via smooth approximation by ABAQUS. In the present study, the FE models of TKD closed-cell foams with corrugated cell walls are generated with w/t equal to 0.25, 0.5, 0.75 and 1. The results shown in Fig. 9 indicate the remarkable influence of cell wall corrugation on creep: the steady state creep rate $\dot{\varepsilon}^*$ increases exponentially, up to a factor of two when w/t reaches 1.

4. Random imperfections

In this section, three types of random imperfections—cell shape irregularity, non-uniform distribution of cell wall thickness, and missing cell walls—are studied. The focus is placed upon identifying morphological imperfections which have a pernicious effect upon creep and thereby providing empirical formulations for predicting the creep response of irregular closed-cell foams. Interactions between the random defects are also addressed. A total of 10 foam samples are analyzed for each case with specific parameters of random imperfections, and only the averaged results are presented.

4.1. Cell shape irregularity

Foam models with cell shape irregularity can be generated by 3D Voronoi tessellation of random distributions of nucleus in the specified space, as demonstrated in refs. [38–40]. In the current study, to obtain periodic boundary conditions, the method outlined in Gan et al. [38,39] is adopted.

For a TKD model with K cells in volume V_0, the minimum distance between any two adjacent nuclei in a regular lattice is given by [41]:

$$d_0 = \frac{\sqrt{6}}{2}\left(\frac{V_0}{\sqrt{2}N}\right)^{\frac{1}{3}} \tag{21}$$

To construct a 3D Voronoi foam model with N cells in V_0, a dimensionless variable α is introduced to represent the degree of cell shape irregularity:

$$\alpha = 1 - \frac{\delta}{d_0} \tag{22}$$

Table 2
Comparison of steady state creep rate of theoretical model predictions with experimental measurements for Alporas foam (average cell size 4.5 mm; relative density 0.088) at $T = 300^{\circ}C$ [18][a].

σ^*(MPa)	$\dot{\varepsilon}^*_{TKD}(s^{-1})$	$\dot{\varepsilon}^*_{CUB}(s^{-1})$	$\dot{\varepsilon}^*_{Exp}(s^{-1})$	$\dot{\varepsilon}^*_{Exp}/\dot{\varepsilon}^*_{TKD}$	$\dot{\varepsilon}^*_{Exp}/\dot{\varepsilon}^*_{CUB}$
0.32	2.56×10^{-10}	2.67×10^{-12}	1.95×10^{-9}	7.62	728
0.40	9.96×10^{-10}	1.08×10^{-11}	6.19×10^{-9}	6.21	573

[a] $\dot{\varepsilon}^*_{TKD}$ and $\dot{\varepsilon}^*_{CUB}$ refer to the predictions of the present TKD closed-cell model (i.e., Eqs. (1), (18) and (19)) and the Gibson-Ashby model (i.e., Eqs. (1) and (2)), respectively; $\dot{\varepsilon}^*_{Exp}$ denotes the experimental results.

where δ is the minimum distance between any two nuclei [38]. With reference to Fig. 10, 5° of cell shape irregularity, i.e., 0.0 (TKD model), 0.25, 0.5, 0.75 and 1.0, are considered in the current study.

Fig. 11a plots the steady state creep rate $\dot{\varepsilon}^*$ as a function of cell shape irregularity α for selected foam relative densities. For each relative density considered, $\dot{\varepsilon}^*$ increases linearly with α. As shown in Fig. 11b, for closed-cell foams with varying cell shape irregularity, the steady state creep rate $\dot{\varepsilon}^*_{ir}$ can be fitted as:

$$\dot{\varepsilon}^*_{ir} = \dot{\varepsilon}^*_{TKD}(1 + I_1\alpha) \tag{23}$$

where $\dot{\varepsilon}^*_{TKD}$ is the steady state creep rate of the regular TKD model ($\alpha = 0$) and the fitting constant $I_1 = 1.35$ regardless of foam relative density.

4.2. Missing cell walls

By randomly removing cell walls (see Fig. 12a) with area fractions d of 1%, 2%, 4%, and 8% from the regular TKD or Voronoi models, the effect of missing cell walls on $\dot{\varepsilon}^*$ is studied, as shown in Fig. 12b. Foam models with the cell shape irregularity α varying as 0, 0.25, 0.5, 0.75 and 1 are considered, and the relative densities of the initially intact models without missing cell walls are fixed at 0.088. Since removing cell walls reduces the relative density, for comparison, $\dot{\varepsilon}^*$ of intact TKD model ($\alpha = 0$) having the same relative densities of $0.088(1 - d)$ as those of models with missing cell walls is also numerically calculated. Upon reducing cell wall thickness t, the reduction in relative density is kept the same as the fraction of random missing cell walls.

The results of Fig. 12b reveal that $\dot{\varepsilon}^*$ increases significantly with increasing d for all the values of α considered. For each α, $\dot{\varepsilon}^*$ increases by about a factor of 2.5 as d is increased from 0 to 0.08. The $\dot{\varepsilon}^*$ versus d curves are essentially parallel, which implies that there is little interaction between the cell shape irregularity and the missing cell walls in term of steady state creep rate. Moreover, it is noted that for the case of $\alpha = 0$, the effect of missing cell walls is much more pronounced than the reduction of relative density, which is also verified for $\alpha \neq 0$ cases (details not shown for brevity).

Further, the steady state creep rate $\dot{\varepsilon}^*_{mis}$ of foam models with miss cell walls normalized by that ($\dot{\varepsilon}^*_{ir}$) of intact models with the same cell shape irregularity is replotted in Fig. 12c. For each value of d, only small scatter of $\dot{\varepsilon}^*_{mis}/\dot{\varepsilon}^*_{ir}$ for models with five different cell shape irregularities is observed, which demonstrates further the little interaction between cell shape irregularity and missing cell walls.

Missing cell walls shed load to the neighboring walls, thus increasing the average effective stress of cell walls [18]. The average effective stress σ^*_{eff} can be written as:

$$\sigma^*_{eff} = \sigma^*_{ir}(1 + I_2 d) \tag{24}$$

where σ^*_{ir} is the average effective stress of the intact TKD ($\alpha = 0$) or Voronoi ($\alpha \neq 0$) foam model, and I_2 is an empirical constant. Therefore,

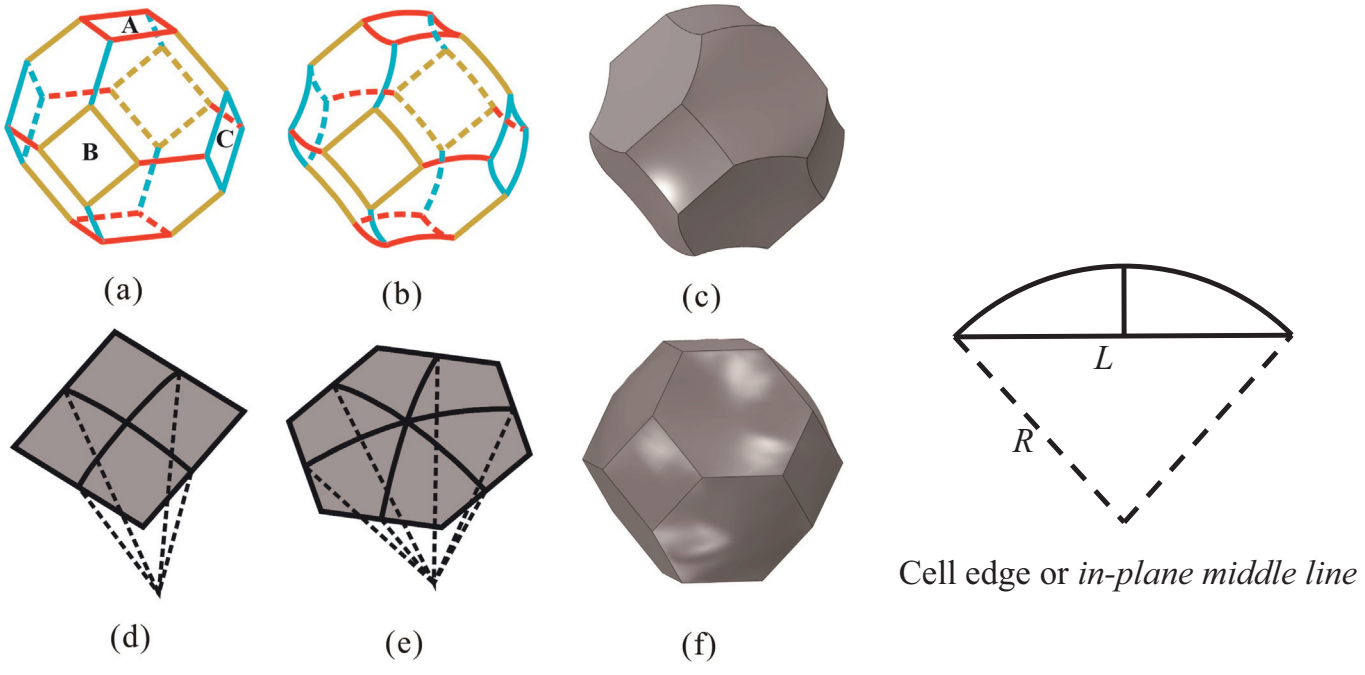

Fig. 6. Construction of curved cell walls determined by the curvature of cell edges and *in-plane middle lines*.

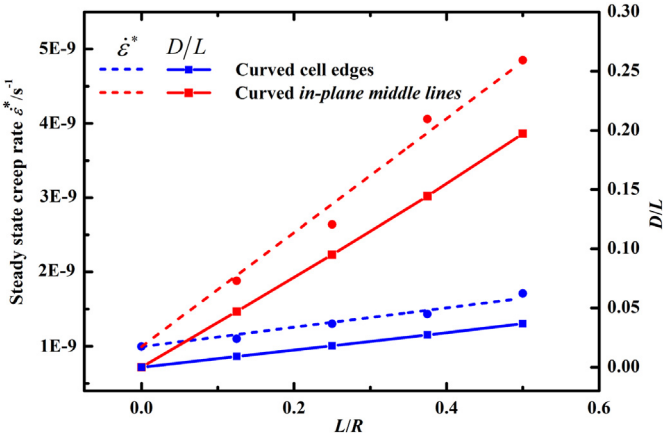

Fig. 7. Steady state creep rate and maximum out-of-plane deflection D (normalized by L) plotted against L/R for TKD closed-cell foams constructed with curved cell edges and curved *in-plane middle lines*. Dash/solid lines refer to the fitting lines, and symbols denote FE simulation results.

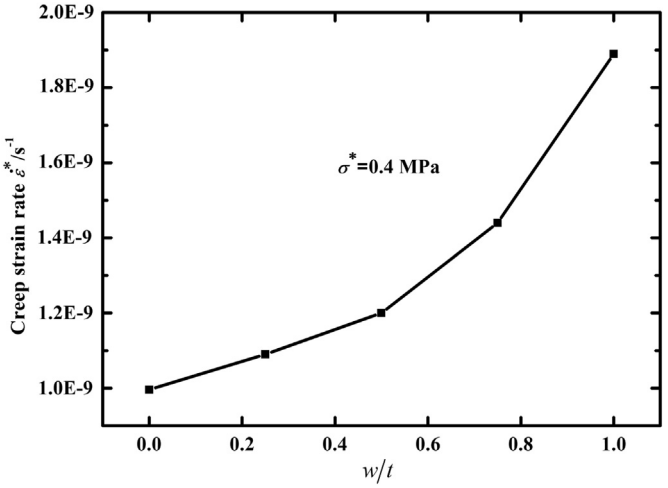

Fig. 9. Steady state creep rate plotted as a function of corrugation amplitude w/t for TKD closed-cell foams with corrugated cell walls.

the steady state creep rate of foams with missing cell walls $\dot{\varepsilon}^*_{mis}$ can be given by:

$$\dot{\varepsilon}^*_{mis} = \dot{\varepsilon}^*_{ir}\left(\frac{\sigma^*_{eff}}{\sigma^*_{ir}}\right)^n = \dot{\varepsilon}^*_{ir}(1+I_2 d)^n \tag{25}$$

Based on fitting the numerical results of Fig. 12c, $I_2 = 2.73$ is obtained using the least squares method.

4.3. Non-uniform distribution of cell wall thickness

Non-uniform distribution of cell wall thickness is commonly found in closed-cell foams [21,31,36] and can affect significantly the stiffness and strength of the foam [25,42]. In this section, the effect of non-uniform distribution of cell wall thickness on foam creep is quantified using the model as illustrated in Fig. 13a. To take into account the statistical dispersion of cell wall thickness, a probabilistic approach is undertaken. To this end, the cell wall thickness t is taken as a stochastic variable, characterized by a probability density function. Upon assuming a normal distribution, the non-uniform distribution of cell wall thickness is approximately described by the scaling of a standardized normally distributed stochastic cell wall thickness, with the probability density function given as:

$$f(t) = \frac{1}{\sqrt{2\pi}\delta} e^{-\frac{(t-t_0)^2}{2\delta^2}} \tag{26}$$

where t_0 is the expectation of cell wall thickness distribution, and δ is the standard deviation reflecting the dispersion of cell wall thickness. Eq. (26) can also be expressed as $t \sim N(t_0, \delta^2)$. The parameter δ/t_0 is introduced to quantify the degree of the dispersity of cell wall thickness, with a smaller δ/t_0 representing a smaller dispersity. After each cell wall is assigned a random thickness, the relative density of the foam model is given by:

$$\overline{\rho} = \left(\sum_j S_j \cdot t_j\right)/V_0 \tag{27}$$

where S_j is the area of cell wall j, t_j is the corresponding wall thickness, and V_0 is the volume of the whole model. Based on the TKD or Voronoi closed-cell model with different cell shape irregularities (α), four normal distributions of cell wall thickness having the same relative density of 0.088 but different values of δ/t_0, i.e., 0.0 (uniform cell wall thickness), 0.2, 0.4 and 0.6, are investigated.

Fig. 13b presents the variation of steady state creep rate $\dot{\varepsilon}^*$ with the variability in δ/t_0 for foam models having different cell shape irregularities (α). It is found that $\dot{\varepsilon}^*$ rises at an increasing rate as the dispersity of cell wall thickness is increased. For each α value, $\dot{\varepsilon}^*$ increases by about 3 times as δ/t_0 is increased from 0 to 0.6. Similar to the finding of Section 4.2, it is also found that the $\dot{\varepsilon}^*$ versus δ/t_0 curves for different cell shape irregularities are approximately parallel to each other. This implies that there is little interaction between cell shape irregularity and non-uniform distribution of cell wall thickness in term of steady state creep rate.

The steady state creep rate of foam models with non-uniform distribution of cell wall thickness $\dot{\varepsilon}^*_{rt}$, normalized by that of models having the same cell shape irregularity but uniform wall thickness $\dot{\varepsilon}^*_{ir}$, is replotted in Fig. 13c. It can be seen that $\dot{\varepsilon}^*_{rt}/\dot{\varepsilon}^*_{ir}$ from the numerical simulations exhibits larger scatter as δ/t_0 increases. This is mainly caused by the fact that the dispersion of cell wall thickness becomes larger for random distribution of cell walls, as δ/t_0 is increased from 0 to 0.6.

The strong dependence of $\dot{\varepsilon}^*$ on δ/t_0 is mainly attributed to thin cell walls whose thickness is smaller than t_0. When subjected to the same

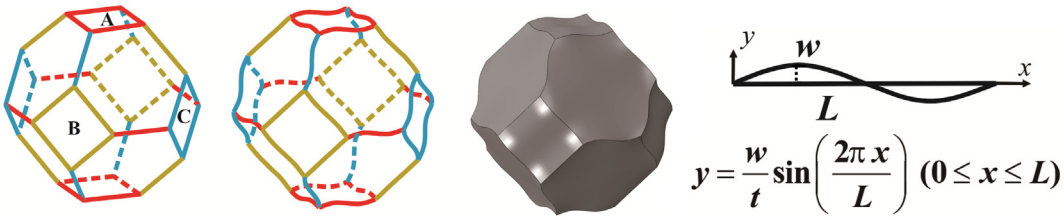

Fig. 8. Construction of corrugation in cell walls using corrugated cell edges.

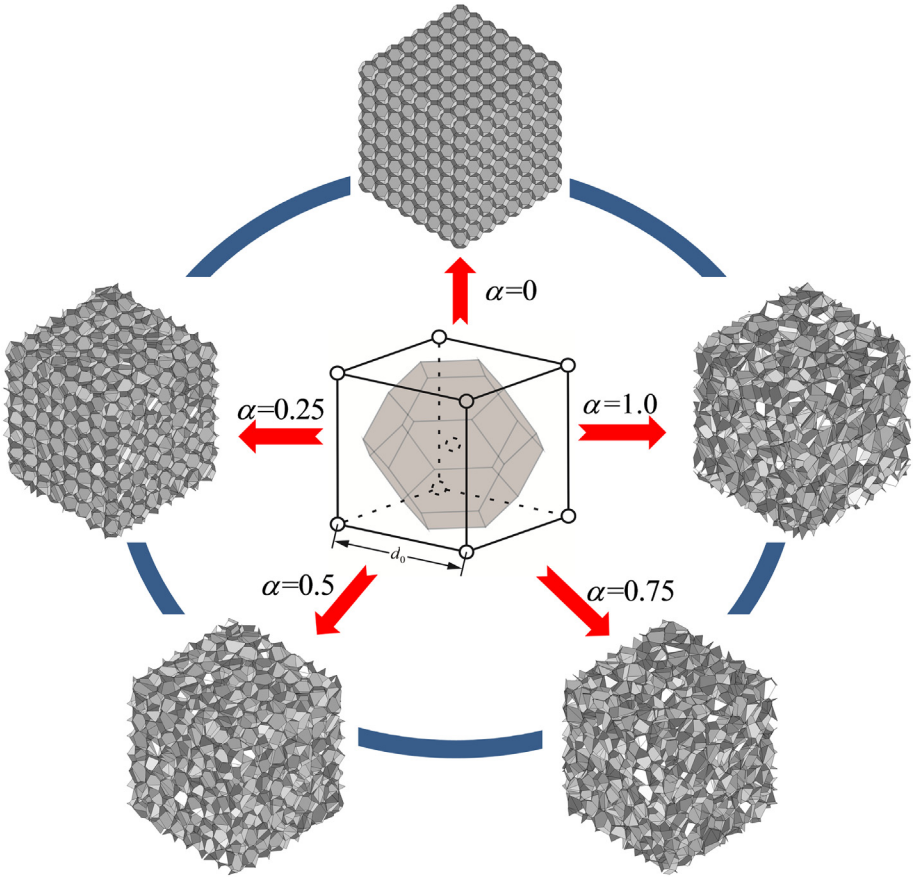

Fig. 10. Construction of TKD and Voronoi closed-cell foam models based on BCC lattice of seeds.

stress, these cell walls will creep faster, thus increasing the creep rate of the whole model. It is assumed that the effect of non-uniform distribution of cell wall thickness may be described by the increasing of average effective stress

$$\sigma^*_{eff} = \sigma^*_{ir}\left[1 + I_3(\delta/t_0)^{\beta}\right] \tag{28}$$

where σ^*_{ir} is the average effective stress of the intact TKD or Voronoi foam model having uniform wall thickness, while I_3 and β are undetermined coefficients. Thus the steady state creep rate of foams with non-uniform distribution of cell wall thickness $\dot{\varepsilon}^*_{rt}$ can be written as:

$$\dot{\varepsilon}^*_{rt} = \dot{\varepsilon}^*_{ir}\left(\frac{\sigma^*_{eff}}{\sigma^*_{ir}}\right)^n = \dot{\varepsilon}^*_{ir}\left[1 + I_3(\delta/t_0)^{\beta}\right]^n \tag{29}$$

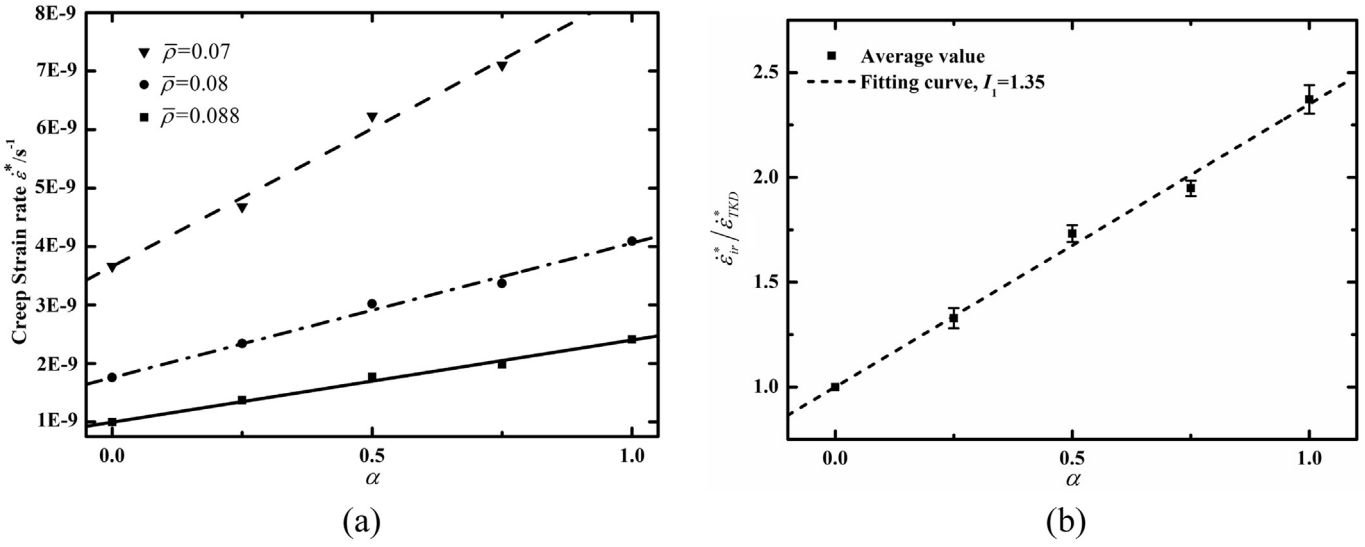

Fig. 11. Effect of cell shape irregularity on steady state creep: (a) creep strain rate plotted as a function of irregularity α for selected relative densities; (b) normalized creep rate $\dot{\varepsilon}^*_{ir}/\dot{\varepsilon}^*_{TKD}$ plotted against α.

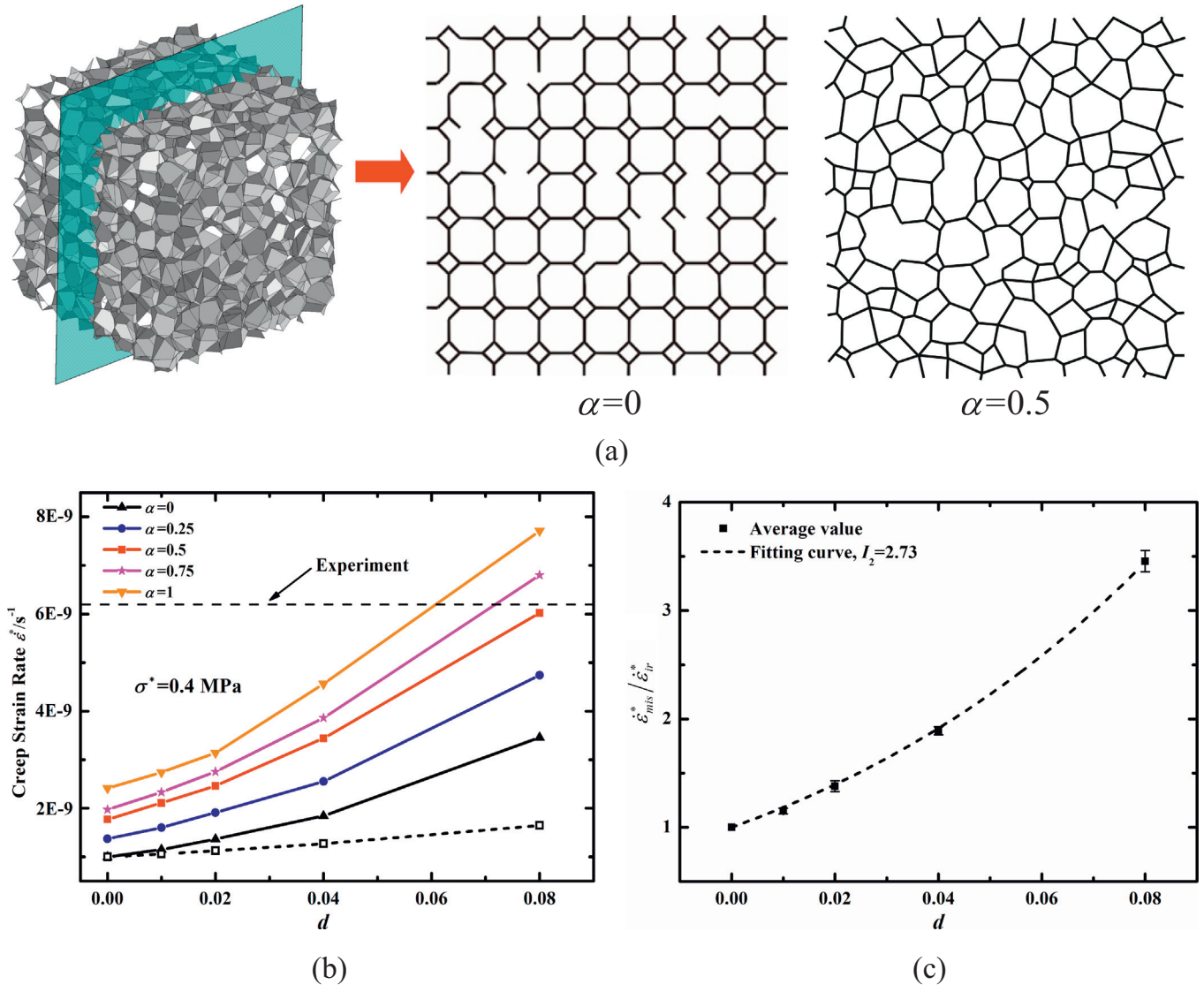

Fig. 12. Effect of missing cell walls on steady state creep: (a) cross-section of foam models containing missing cell walls for both regular TKD and Voronoi models; (b) steady state creep rate plotted as a function of area fraction of random missing cell walls d for selected values of irregularity α; (c) normalized creep rate $\dot{\varepsilon}^*_{mis}/\dot{\varepsilon}^*_{int}$ plotted against d. For panel b, reference line for TKD ($\alpha = 0$) with the relative density of $0.88(1-d)$ is added as the dash line with hollow square symbols.

Based on fitting with the numerical results from Fig. 13c, the values of I_3 and β can be determined as 0.51 and 1.36 by the least squares method.

4.4. Coexistence of cell shape irregularity, missing cell walls and non-uniform distribution of cell wall thickness

In real foams, random defects such as cell shape irregularity, missing cell walls and non-uniform distribution of wall thickness often exist simultaneously. To investigate their combined effect, 3D Voronoi tessellation models with simultaneous missing cell walls and non-uniform distribution of wall thickness are employed, as shown in Fig. 14.

To construct the FE models that contain simultaneously the three random defects, the 3D Voronoi closed-cell foam model with cell shape irregularity of α and relative density of 0.088 is firstly set up. Subsequently, cell walls with an area fraction of d are randomly removed. Finally, cell wall thickness with non-uniform distribution of dispersity δ/t_0 is randomly allocated to the remaining cell walls. In this section, six foam models with three different random imperfections are constructed to calculate the steady state creep rate, and the results are summarized in Table 3.

By comparing the results of Table 3, Figs. 12b and 13b, it is found that the combined effect of the random defects considerably weakens the foam, causing more drastic increase in steady state creep rate relative to that of any single or dual imperfections. It can be supposed that, together, the three random imperfections cause inhomogeneous distribution of stresses in the foam, and hence accelerate creep in high stress regions to influence the overall creep rate.

As discussed previously, interaction between missing cell walls and cell shape irregularity, and that between non-uniform distribution of wall thickness and cell shape irregularity are both weak and can be ignored. Additionally assuming that there is little interaction between missing cell walls and non-uniform distribution of wall thickness, and incorporating Eqs. (1), (18), (19), (23), (25) and (29), one may approximately express the steady state creep rate of closed-cell foams containing all the three random defects as

$$\dot{\varepsilon}^*_{imp} = \dot{\varepsilon}^*_0 \left(\frac{\sigma^*}{\sigma_0}\right)^n \left[A_1(\phi\overline{\rho})^{\frac{3n+1}{2n}} + A_2(1-\phi)\overline{\rho}\right]^{-n} (1+I_1\alpha)(1+I_2 d)^n \left[1+I_3(\delta/t_0)^{\beta}\right]^n \tag{30}$$

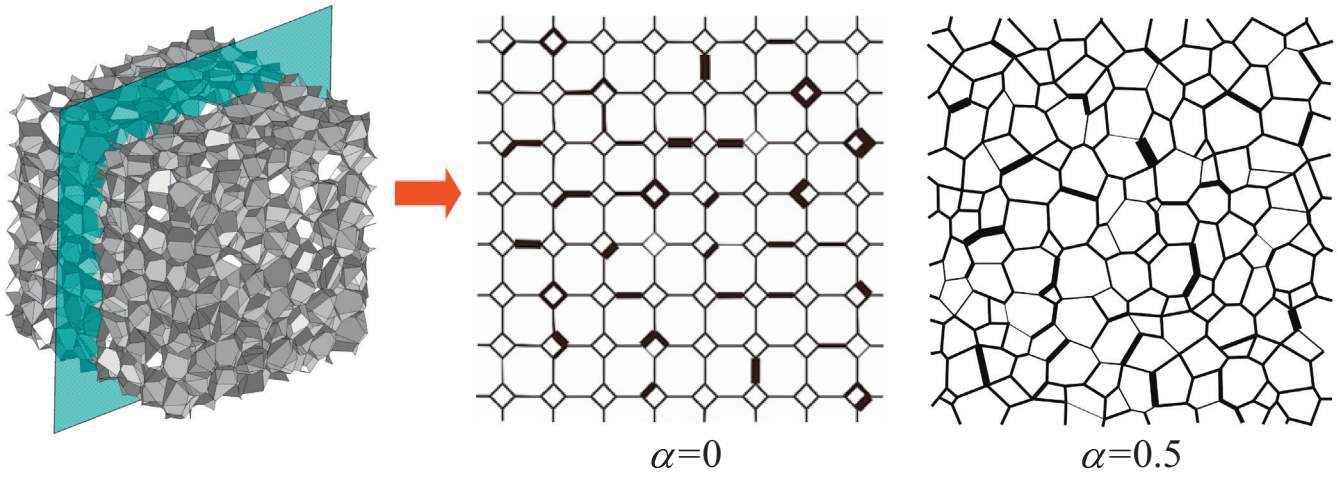

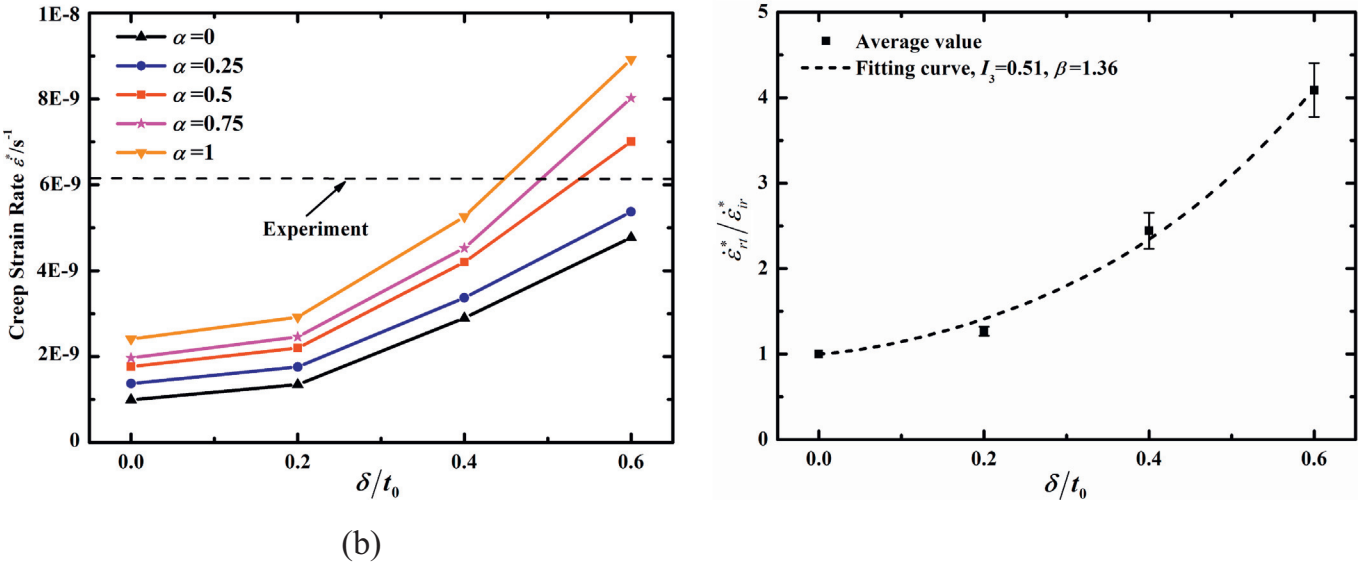

Fig. 13. Effect of non-uniform distribution of cell wall thickness on steady state creep: (a) cross-sections of foam models; (b) steady state creep rate plotted as a function of δ/t_0 for selected values of α; (c) normalized creep rate $\dot{\varepsilon}^*_{rt}/\dot{\varepsilon}^*_{ir}$ plotted as a function of δ/t_0.

where A_1 and A_2 are constants as determined in Section 2.3, and I_1, I_2, I_3 and β are constants equal to 1.35, 2.73, 0.51 and 1.36, which are also determined previously. It is noteworthy that $\overline{\rho}$ refers to the relative density of the initial intact foams without missing cell walls, while the actual relative density of foams with missing cell walls is $\overline{\rho}(1-d)$.

It can be seen from Table 3 that the predicted results by the empirical formula of Eq. (30) agree well with those from numerical simulations. This implies that the mutual interactions among the three random defects are small as far as their effects on steady state creep rate are of concern.

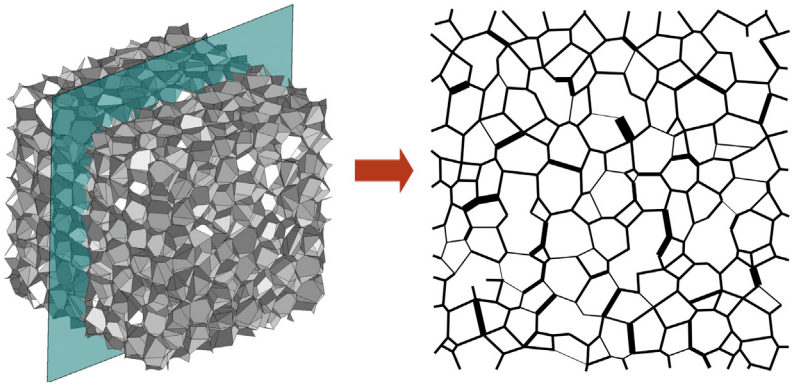

Fig. 14. Illustration of 3D closed-cell foam models containing simultaneously three types of random defects: cell shape irregularity, missing cell walls, and non-uniform distribution of cell wall thickness.

Table 3
Steady state creep rate of closed-cell foam models containing simultaneously three random defects: comparison between empirical formula and FE simulation[a].

α	d	δ/t	$\dot{\varepsilon}^*_{Anl}(s^{-1})$	$\dot{\varepsilon}^*_{FE}(s^{-1})$	$\Delta(\%)$
0	0	0	9.96×10^{-10}	–	–
0.25	0.04	0.4	5.99×10^{-9}	5.68×10^{-9}	5.5
0.5	0.02	0.4	5.47×10^{-9}	5.56×10^{-9}	−1.6
0.5	0.04	0.4	7.50×10^{-9}	7.02×10^{-9}	6.8
0.5	0.08	0.4	1.35×10^{-8}	1.41×10^{-8}	−4.3
0.75	0.04	0.4	9.01×10^{-9}	8.26×10^{-9}	9.1
0.75	0.04	0.6	1.58×10^{-8}	1.42×10^{-8}	11.3

[a] $\dot{\varepsilon}^*_{Anl}$ and $\dot{\varepsilon}^*_{FE}$ refer to the steady state creep rate of closed-cell foams obtained from Eq. (30) and FE simulations, respectively. Δ denotes the percentage error of $\dot{\varepsilon}^*_{Anl}$ relative to $\dot{\varepsilon}^*_{FE}$. The case without defects is added as a reference.

5. Conclusions

The effects of cell-wall imperfections, including curved walls, corrugation, cell shape irregularity, missing walls and non-uniform distribution of wall thickness, on steady-state creep of closed-cell aluminum foams are studied numerically and analytically. A refined theoretical model is firstly developed to predict the creep rate of idealized TKD closed-cell foams. Subsequently, the effects of periodic imperfections and random imperfections are separately studied via FE simulations. Finally, based on the simulation results, an empirical formula is proposed to predict the steady state creep rate of closed-cell foams containing random imperfections. The main conclusions are:

(1) The steady state creep rate of closed-cell aluminum foams mainly depends on the relative density, the geometries, the morphological imperfections, and the creep properties of the parent material.
(2) Whereas the TKD model gives much better predictions than the Gibson-Ashby model, both predictions greatly underestimate the steady state creep rate of closed-cell foams because the effects of morphological defects on creep are not considered in the models.
(3) Considered as periodic imperfections, curved cell walls usually lead to a linear increase of creep rate, while corrugated cell walls cause an exponential increase. Curved cell walls caused by curved cell edges are more prone to creep than those caused by curved *in-plane middle lines*.
(4) As random defects, cell shape irregularity, missing cell walls, and non-uniform distribution of cell wall thickness can all accelerate creep significantly: the creep rate increases linearly with cell shape irregularity, but varies as a power-law function of the area fraction of missing cell walls or the dispersity degree of cell wall thickness.
(5) The combined effect of all three random defects leads to more drastic increase in creep rate than that of any single or dual imperfections, although there is little interaction among the three random defects. The proposed empirical formula gives a good prediction of closed-cell foam models with random defects, and can be used to approximately predict the steady state creep rate of closed-cell aluminum foams in practice.

Acknowledgments

This work was supported by the National Natural Science Foundation of China (51375369, 11472209, and 11472208), China Postdoctoral Science Foundation (2016M600782), Postdoctoral Scientific Research Project of Shaanxi Province (2016BSHYDZZ18), Zhejiang Provincial Natural Science Foundation of China (LGG18A020001) and the Fundamental Research Funds for Xi'an Jiaotong University (xjj2015102).

References

[1] M.F. Ashby, A. Evans, N.A. Fleck, L.J. Gibson, J.W. Hutchinson, H.N.G. Wadley, Metal Foams: A Design Guide, Butterworth-Heinemann, Oxford, 2000.
[2] J. Banhart, Manufacture, characterisation and application of cellular metals and metal foams, Prog. Mater. Sci. 46 (6) (2001) 559–632.
[3] H. Nakajima, Fabrication, properties and application of porous metals with directional pores, Prog. Mater. Sci. 52 (7) (2007) 1091–1173.
[4] S.M. Oppenheimer, D.C. Dunand, Finite element modeling of creep deformation in cellular metals, Acta Mater. 55 (11) (2007) 3825–3834.
[5] A.C.F. Cocks, M.F. Ashby, Creep-buckling of cellular solids, Acta Mater. 48 (13) (2000) 3395–3400.
[6] E.W. Andrews, L.J. Gibson, The role of cellular structure in creep of two-dimensional cellular solids, Mater. Sci. Eng. A 303 (1–2) (2001) 120–126.
[7] J.S. Huang, L.J. Gibson, Creep of open-cell Voronoi foams, Mater. Sci. Eng. A 339 (1–2) (2003) 220–226.
[8] T.J. Chen, J.S. Huang, Creep-rupturing of cellular materials: regular hexagonal honeycombs with dual imperfections, Compos. Sci. Technol. 68 (6) (2008) 1562–1569.
[9] R.K. Oruganti, A.K. Ghosh, FEM analysis of transverse creep in honeycomb structures, Acta Mater. 56 (4) (2008) 726–735.
[10] Y. Boonyongmaneerat, D.C. Dunand, Effects of strut geometry and pore fraction on creep properties of cellular materials, Acta Mater. 57 (5) (2009) 1373–1384.
[11] Z.G. Fan, C.Q. Chen, T.J. Lu, Multiaxial creep of low density open-cell foams, Mater. Sci. Eng. A 540 (2012) 83–88.
[12] A. Burteau, J.D. Bartout, Y. Bienvenu, S. Forest, On the creep deformation of nickel foams under compression, C. R. Phys. 15 (8–9) (2014) 705–718.
[13] B.Y. Su, Z.W. Zhou, Z.H. Wang, Z.Q. Li, X.F. Shu, Effect of defects on creep behavior of cellular materials, Mater. Lett. 136 (2014) 37–40.
[14] B.Y. Su, Z.W. Zhou, X.F. Shu, Z.H. Wang, Z.Q. Li, L.M. Zhao, Multiaxial creep of transversely isotropic foams, Mater. Sci. Eng. A 658 (2016) 289–295.
[15] K. Kwok, D. Boccaccini, A.H. Persson, H.L. Frandsen, Homogenization of steady-state creep of porous metals using three-dimensional microstructural reconstructions, Int. J. Solids Struct. 78-79 (2016) 38–46.
[16] L.J. Gibson, M.F. Ashby, Cellular Solids: Structure and Properties, 2nd ed. Cambridge University Press, New York, 1997.
[17] E.W. Andrews, L.J. Gibson, M.F. Ashby, The creep of cellular solids, Acta Mater. 47 (10) (1999) 2853–2863.
[18] E.W. Andrews, J.S. Huang, L.J. Gibson, Creep behavior of a closed-cell aluminum foam, Acta Mater. 47 (10) (1999) 2927–2935.
[19] P. Zhang, M. Haag, O. Kraft, A. Wanner, E. Arzt, Microstructural changes in the cell walls of a closed-cell aluminium foam during creep, Philos. Mag. A 82 (16) (2002) 2895–2907.
[20] M. Haag, A. Wanner, H. Clemens, P. Zhang, O. Kraft, E. Arzt, Creep of aluminum-based closed-cell foams, Metall. Mater. Trans. A 34 (12) (2003) 2809–2817.
[21] C. Chen, T.J. Lu, N.A. Fleck, Effect of imperfections on the yielding of two-dimensional foams, J. Mech. Phys. Solids 47 (11) (1999) 2235–2272.
[22] I. Jeon, T. Asahina, The effect of structural defects on the compressive behavior of closed-cell Al foam, Acta Mater. 53 (12) (2005) 3415–3423.
[23] Y.L. Sun, X. Zhang, Z.S. Shao, Q.M. Li, Image-based correlation between the meso-scale structure and deformation of closed-cell foam, Mater. Sci. Eng. A 688 (2017) 27–39.
[24] F. Gagliardi, L. De Napoli, L. Filice, D. Umbrello, A comparison among FE models to simulate metallic foams forming - an experimental validation, Mater. Des. 30 (4) (2009) 1282–1287.
[25] Y.M. Chen, R. Das, M. Battley, Effects of cell size and cell wall thickness variations on the stiffness of closed-cell foams, Int. J. Solids Struct. 52 (2015) 150–164.
[26] Y.L. Sun, Q.M. Li, T. Lowe, S.A. McDonald, P.J. Withers, Investigation of strain-rate effect on the compressive behaviour of closed-cell aluminium foam by 3D image-based modelling, Mater. Des. 89 (2016) 215–224.
[27] M.A. Kader, M.A. Islam, M. Saadatfar, P.J. Hazell, A.D. Brown, S. Ahmed, J.P. Escobedo, Macro and micro collapse mechanisms of closed-cell aluminium foams during quasi-static compression, Mater. Des. 118 (2017) 11–21.
[28] J.Y. Lin, J.S. Huang, Creep of hexagonal honeycombs with plateau borders, Compos. Struct. 67 (4) (2005) 477–484.
[29] A.E. Simone, L.J. Gibson, Aluminum foams produced by liquid-state processes, Acta Mater. 46 (9) (1998) 3109–3123.
[30] T.J. Lu, Q.C. Zhang, F. Jin, Resent progress in the development of lightweight porous materials and structures, Mater. China 31 (1) (2012) 13–34.
[31] K. Li, X.L. Gao, G. Subhash, Effects of cell shape and cell wall thickness variations on the elastic properties of two-dimensional cellular solids, Int. J. Solids Struct. 42 (5–6) (2005) 1777–1795.
[32] D. Weaire, M.A. Fortes, Stress and strain in liquid and solid foams, Adv. Phys. 43 (6) (1994) 685–738.

[33] A.E. Simone, L.J. Gibson, Effects of solid distribution on the stiffness and strength of metallic foams, Acta Mater. 46 (6) (1998) 2139–2150.
[34] S.K. Nammi, G. Edwards, H. Shirvani, Effect of cell-size on the energy absorption features of closed-cell aluminium foams, Acta Astronaut. 128 (2016) 243–250.
[35] K. Li, X.L. Gao, A.K. Roy, Micromechanics model for three-dimensional open-cell foams using a tetrakaidecahedral unit cell and Castigliano's second theorem, Compos. Sci. Technol. 63 (12) (2003) 1769–1781.
[36] A.E. Simone, L.J. Gibson, The effects of cell face curvature and corrugations on the stiffness and strength of metallic foams, Acta Mater. 46 (11) (1998) 3929–3935.
[37] N.C. Fahlbusch, G.L. Grenestedt, W. Becker, Effective failure behavior of an analytical and a numerical model for closed-cell foams, Int. J. Solids Struct. 97-98 (2016) 417–430.
[38] Y.X. Gan, C. Chen, Y.P. Shen, Three-dimensional modeling of the mechanical property of linearly elastic open cell foams, Int. J. Solids Struct. 42 (2005) 6628–6642.
[39] Y.Z. Song, Z.H. Wang, L.M. Zhao, J. Luo, Dynamic crushing behavior of 3D closed-cell foams based on Voronoi random model, Mater. Des. 31 (2010) 4281–4289.
[40] Z.Q. Li, J.J. Zhang, J.H. Fan, Z.H. Wang, L.M. Zhao, On crushing response of the three-dimensional closed-cell foam based on Voronoi model, Mech. Mater. 68 (2014) 85–94.
[41] H.X. Zhu, J.R. Hobdell, A.H. Windle, Effects of cell irregularity on the elastic properties of open-cell foams, Acta Mater. 48 (20) (2000) 4893–4900.
[42] Y.M. Chen, R. Das, M. Battley, Effects of cell size and cell wall thickness variations on the strength of closed-cell foams, Int. J. Eng. Sci. 120 (2017) 220–240.